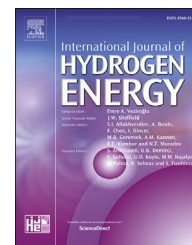


Available online at www.sciencedirect.com

ScienceDirect

journal homepage: www.elsevier.com/locate/he

A computational study of hydrogen adsorption on penta-NiN₂ sheet and nanotubes



Ahmed H. Ati^a, Jiewei Cheng^a, Qiang Sun^{a,b,*}

^a School of Materials Science and Engineering, Peking University, Beijing 100871, China

^b Center for Applied Physics and Technology, Peking University, Beijing 100871, China

HIGHLIGHTS

- Penta-sheet and nanotube for hydrogen storage.
- Each Ni site in the penta-NiN₂ sheet can only adsorb two H₂ molecules.
- The perfect penta-NiN₂ sheet can't reach the DOE target for H₂ storage.
- N-vacancy, Ni replacement, and grain boundary need to be introduced to enhance the adsorption energy and capacity.

ARTICLE INFO

Article history:

Received 4 January 2023

Received in revised form

18 April 2023

Accepted 11 June 2023

Available online 27 June 2023

Keywords:

Penta-NiN₂ sheet and nanotubes

Hydrogen storage

Van der Waals-corrected DFT

Desorption temperature

ABSTRACT

Stimulated by the recent synthesis of penta-NiN₂ sheet [ACS Nano 2021, 15, 13,539], we study the hydrogen adsorption on the sheet and the derived nanotubes by using density functional theory with the correction of van der Waals interactions. We have found that each Ni site can only adsorb two hydrogen molecules as expected from the 18-electron rule, the corresponding capacity is 4.44 wt%. As more H₂ molecules are introduced, H₂ can only be very weakly adsorbed on N sites. When the sheet is curved into nanotubes, the Ni–N distance is enlarged due to the stress, which weakens the orbital hybridizations between Ni and N, and reduces the charge transfer from Ni to N. The Ni ion with a less charge on the tube shows weak polarizing ability for H₂ molecule.

© 2023 Hydrogen Energy Publications LLC. Published by Elsevier Ltd. All rights reserved.

Introduction

Solid materials for hydrogen storage via absorption and adsorption are of current interest as required by the green renewable energy technology. Materials suitable for hydrogen storage must meet specific requirements, such as an optimal adsorption energy window (0.1–0.6 eV/H₂) [1], and high gravimetric (5.5%) and volumetric (40 g/L) capacity targets set by the United States Department of Energy [2]. However, it is

challenging to reach these targets, which motivates scientists to design new materials.

Since the proposal of penta-graphene (PG) [3], pentagon becomes an important structural unit that has led to a paradigm shift in new materials design and synthesis. So far, more than 150 penta-sheets have been proposed [4] exhibiting unique geometry and novel properties as compared with graphene, MXene, black phosphorus, dichalcogenides, and trichalcogenides. Pentagon-based 2D sheets significantly expanded the 2D materials family with additional new

* Corresponding author. School of Materials Science and Engineering, Peking University, Beijing 100871, China.

E-mail address: sunqiang@pku.edu.cn (Q. Sun).

<https://doi.org/10.1016/j.ijhydene.2023.06.120>

0360-3199/© 2023 Hydrogen Energy Publications LLC. Published by Elsevier Ltd. All rights reserved.

features for many potential applications. One of them is for hydrogen storage [5]. For example, Zhang et al. found that Li-decorated double-sided penta-silicene could achieve an average adsorption energy of -0.22 eV/H₂ and a hydrogen uptake capacity of 6.42 wt% [6]; Hao et al. also studied lithium-decorated nitrogen-doped PG and observed gravimetric densities of up to 7.88 wt% with average adsorption energies within the range of physical adsorption processes (0.1–0.4 eV) [7]; Shajahan et al. explored zirconium-decorated PG with an average adsorption energy of -0.42 eV, where electrons were transferred from Zr 3d orbital to hydrogen 1s orbital, followed by back donation from H 1s to Zr 3d orbital, leading to a gravimetric hydrogen uptake of 14.8 wt% [8]; Bi et al. examined penta-octa-graphene adorned with various metals and demonstrated that Li and Ti could adsorb up to 3 and 5 hydrogen molecules, respectively, resulting in gravimetric capacities of up to 9.9 wt% and 6.5 wt% [9]. Additionally, Ma et al. identified Li-doped defective CN₂ sheets as having a high hydrogen storage capacity of up to 10.90 wt% [10]. However, in all these theoretical predictions of the hydrogen storage on penta-sheets reported so far, none of the sheets have been synthesized. Among the synthesized 2D pentagonal sheets, penta-NiN₂ is the first system synthesized with high pressure [11], where Ni is intrinsically in the structure, there is no need to introduce metal doping and avoided the clustering problem. In addition, Ni atoms have been widely introduced to C₆₀, BN cage, SiC cage, BN sheet and BN nanotube for H₂ storage [12–17]. Furthermore, the Ni-dihydrogen complex has been observed in experiment [18]. These research advances motivate us to carry out this study on exploring H₂ adsorption on penta-NiN₂ monolayer and its nanotubes.

Computational details

All computations are performed using density functional theory as implemented in the Vienna *ab initio* simulation (VASP) package [19]. The electron-ion interactions are described using the projector augmented wave approach [20] with energy cutoff of 550 eV, and the electron exchange-correlation interactions are treated with Perdew-Burke-Ernzerhof functional [21] for geometry optimization, and HSE06 hybrid density functional [22] is employed for an accurate electronic band structure, while the semi-empirical Grimme (DFT-D3) dispersion correction is applied to account for long-range interactions in adsorption [23]. The Brillouin Zone (BZ) is sampled using the Monkhorste-Pack approach with mesh of $5 \times 10 \times 1$ and $1 \times 1 \times 8$ for the monolayer and nanotubes, respectively [24]. The convergence criterion is 10^{-7} eV and 0.01 eV/Å for energy and force, respectively. To avoid image interactions due to periodicity, a vacuum space of 15 Å is introduced in the out-of-plane direction along the z-axis for the monolayer and along the x- and y-axis for nanotubes. The dynamic stability of the nanotubes is verified via vibrational spectrum simulations, and the energetic stability is checked by formation energy from the monolayer [25]:

$$E_{\text{str}} = \left[\frac{E_{\text{NT}}}{n_{\text{NT}}} - \frac{E_{\text{slab}}}{n_{\text{slab}}} \right] \quad (1)$$

where E_{NT} , E_{slab} are the total energy, and n is the number of chemical formula units in the nanotube and slab supercell, respectively.

The maximum adsorbed hydrogen molecules on transition metal site are typically determined using 18-electron rule [26–28], as the following:

$$n = \left[\frac{18 - n_v - 4}{2} \right] \quad (2)$$

where n is the maximum number of adsorbed H molecules, n_v is the number of valence electrons of metal atom (here Ni), and 4 is the number of electrons contributed by the ring (the number of Ni–N bonds in the pentagonal ring).

The average adsorption energy (E_{ads}) is defined as [29–31]:

$$E_{\text{ads}} = \frac{\{E_{\text{system}} - E_{\text{adsorbent}} - nE_{\text{H}_2}\}}{n} \quad (3)$$

where E_{system} and $E_{\text{adsorbent}}$ are the energy of the whole adsorption system with/without hydrogen molecules and E_{H_2} is the total energy of the free H₂ molecule calculated in a big box, where ($a = b = c = 15$ Å) with Γ -point sampling in BZ.

The gravimetric hydrogen capacity (wt%) is calculated as:

$$\text{wt \%} = \left[\frac{nM_{\text{H}_2}}{nM_{\text{H}_2} + M_{\text{NiN}_2}} \right] \times 100\% \quad (4)$$

where M_{H_2} and M_{NiN_2} are the mass of hydrogen molecules adsorbed and *p*-NiN₂ system adsorbent, respectively.

The desorption temperature (T_d) is calculated from the Vant-Hoff equation [32], as the following:

$$T_d = \frac{|E_{\text{ads}}|}{k_B} \left[\frac{\Delta S}{R} - \ln(P) \right]^{-1} \quad (5)$$

where k_B is the Boltzmann constant (1.38×10^{-23} J/K), ΔS denotes the change in H₂ entropy from the gas to liquid phase (75.44 J/mol.K) [33–36], R is the gas constant (8.314 J/mol.K) and P is the equilibrium pressure, which is selected to be 1 atm.

Results and discussions

Geometries and electronic properties of the penta-NiN₂ sheet and the derived nanotubes

The penta-NiN₂ monolayer has the space group of P4-mpm (IT number: 127) with the optimized lattice constant of $a = b = 4.531$ Å as shown in Fig. 1a, where the Ni–N and N–N bond lengths are 1.878 and 1.243 Å, respectively, which agree well with previous studies [11, 37]. In terms of electronic properties, calculation at PBE level suggests a narrow energy gap of 0.04 eV, which becomes 1.10 eV at HSE06 level as shown in Fig. 1b.

Penta-NiN₂ nanotubes are built by rolling the optimized penta-NiN₂ monolayer for different chiral indices (4, 0), (5, 0), and (8, 0), as illustrated in Fig. 2. The Ni–N and N–N bond lengths in nanotubes are elongated or compressed under the influence of curvature as listed in Table 1. As the tube diameter D increases, the bond lengths approach to that of monolayer as expected.

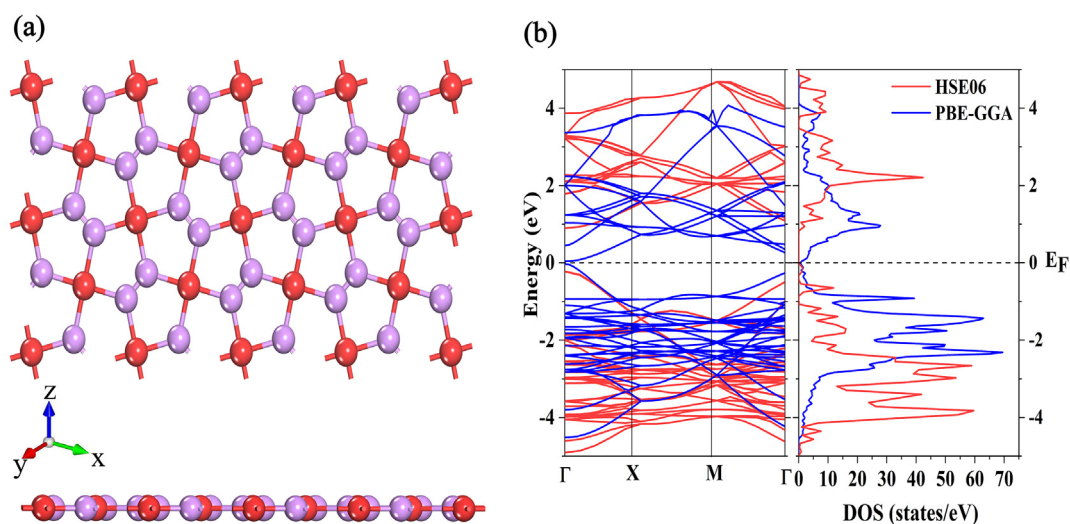


Fig. 1 – (a) Top and side views of the optimized monolayer p -NiN₂ in $4 \times 2 \times 1$ supercell, (b) the electronic band structure and total density of states of the p -NiN₂ monolayer system. The Fermi level (E_F) is set to zero. The red and pink spheres represent Ni and N atoms, respectively. (For interpretation of the references to colour in this figure legend, the reader is referred to the Web version of this article.)

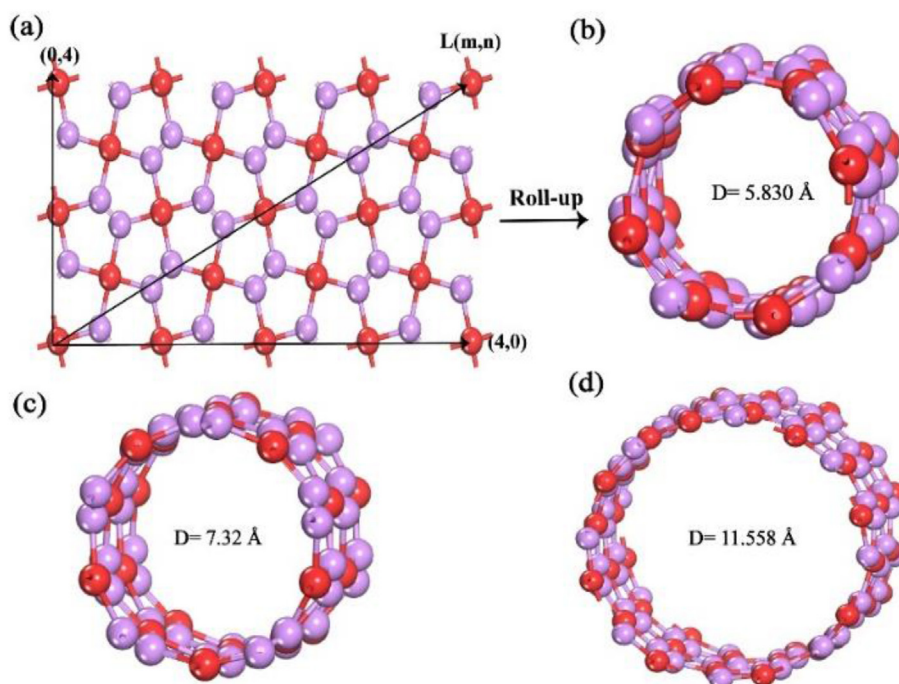


Fig. 2 – (a) Rolling up penta-NiN₂ monolayer into nanotubes with various chiral indices, (b) zigzag tube of (4, 0); (c) (5, 0); (d) (8, 0).

Table 1 – The lattice constant (\AA), bond lengths ($d_{\text{Ni-N}}$) and ($d_{\text{N-N}}$) in (\AA), diameter (D) (\AA), and strain energy E_{str} (eV) of the p -NiN₂ nanotubes (4, 0), (5, 0), and (8, 0).

Chirality	$a = b$ (\AA)	c (\AA)	D (\AA)	$d_{\text{Ni-N}}$ (\AA)	$d_{\text{N-N}}$ (\AA)	E_{str} (eV)
(4, 0)	21.90	4.53	5.83	1.901	1.235	0.117
(5, 0)	22.98	4.54	7.32	1.884	1.246	0.134
(8, 0)	28.35	4.53	11.55	1.881	1.242	0.085

To check the dynamic stability of the nanotubes, phonon spectra are calculated as plotted in Fig. 3, where there are no imaginary phonon modes in the (4, 0) and (8, 0) nanotubes, while (5, 0) shows slight negative mode due to a numerical error in frequency calculation of low-dimensional, which would not affect our judgment about the stability of this material. We also performed a calculation of the strain energy in Equation (1) to evaluate the energetic stability. Because of the stronger curvature effect, penta-NiN₂ nanotubes show

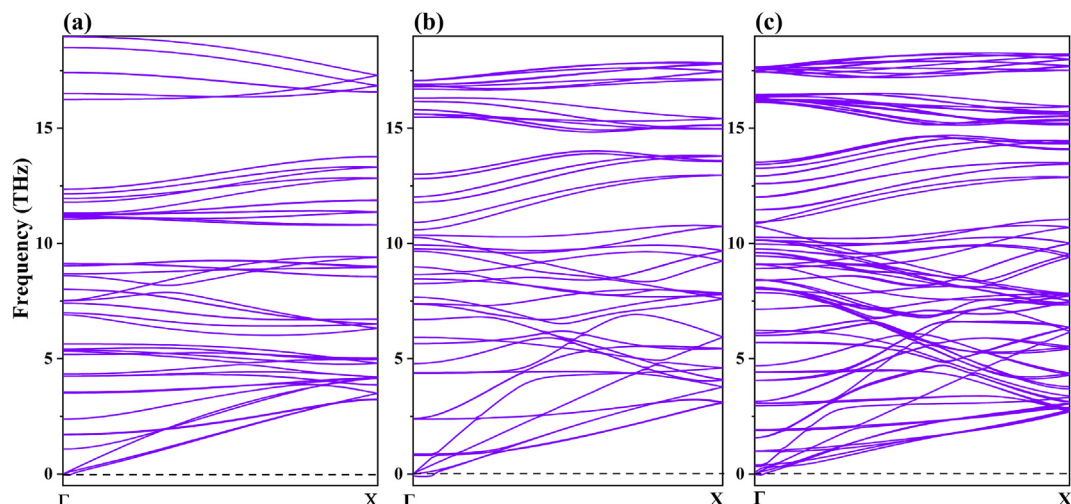


Fig. 3 – Phonon dispersion of the zigzag NTs-NiN₂: (a) (4, 0); (b) (5, 0); (c) (8, 0).

positive strain energies, suggesting that the penta-NiN₂ monolayer is energetically more stable than the nanotubes, see Table 1.

The electronic band structures of nanotubes are further studied as shown in Fig. 4, displaying semiconducting features with bandgap of 0.321, 0.343, and 0.07 eV at PBE level, and 0.57, 1.41 and 1.01 eV at HSE06 level for (4, 0), (5, 0), and (8, 0) NTs, respectively. The valence band maximum and conduction band minimum of NTs (4, 0) and (8, 0) are located at X and Γ points, respectively, while in nanotube (5, 0) the valence band maximum and conduction band minimum are between Γ and X points, see Fig. 4b-d. Due to the decrease in curvature with increases diameter D , the band gap of NTs (8,0) already approaches to that of penta-NiN₂ sheet, indicating that the band gap converges quickly from tube to sheet.

Hydrogen adsorption

In this section, we first study the hydrogen adsorption on the penta-NiN₂ sheet. In the initial structure, hydrogen molecules were placed in side-on configuration on Ni sites. We have tested three cases: (1) 1–0 configuration: one H₂ on one-Ni site at one side; (2) 1-1 configuration: one H₂ on one-Ni site at two sides; (3) 2–1 configuration: two H₂ at one side and one H₂ at the other side. When fully optimized, all the side-on configurations become end-on configurations, as shown in Fig. 5. In 1–0 configuration, the equilibrium distance between H₂ and the sheet is 2.566 Å, the adsorption energy per H₂ is 102.8 meV, based on the Bader charge analysis about 0.006 electrons are transferred to the antibonding orbital of H₂ molecule, which activates the H–H bond to be 0.754 Å; In 1-1 configuration, the corresponding values are 2.632 Å, 102.1 meV, 0.005 and 0.754 Å, and the capacity is 4.44 wt%. While for the optimized 2–1 configuration, two H₂ molecules are on one Ni site in end-on configuration with 2.606 Å from the substrate, and one H₂ molecule is on N–N bridge site with 4.97 Å from the sheet. Namely, the maximum number of adsorbed hydrogen

molecule on each Ni site is two, which is in agreement with the 18-electron rule as stated in Equation (2). Because of this reason, the average adsorption energy is significantly reduced to 63.4 meV. One can see that from 1–0, to 1-1 and 2–1 configurations, as the number of H₂ molecule increases, the adsorption becomes weaker. Accordingly, the desorption temperature decreases from 131 to 130 and 115 K, as shown in Table 2.

Next, we take (4,0) nanotube as an example to study the H₂ adsorption. There are outside and inside surfaces in the nanotube. Due to the small radius, the inside surface doesn't have enough space for H₂. Here we only consider the adsorption on the outside surface. Similar to the configuration labelling in the sheet discussed above, we also test three configurations: (1) 1–0 configuration: one H₂ on each Ni site on the outside surface; (2) 2–0 configuration: two H₂ on each Ni site on the outside surface; (3) 3-0-configuration: three H₂ on each Ni site on the outside surface. For the fully optimized structures as shown in Fig. 6, we found that in the 1–0 and 2–0 configurations, the adsorption distance is 2.808 and 2.863 Å, respectively. The corresponding adsorption energy is 82.1 and 71.6 meV. While in 3–0 configuration, due to the steric hindrance between H₂ molecules, the adsorbed H₂ molecules form two layers with distance of 2.912 and 5.20 Å to the tube outside surface, namely, each Ni site can only adsorb two H₂ molecules as restricted by the 18-electron rule. The calculated parameters are listed in Table 2. When compared with the situation of the sheet, the adsorption of H₂ on the (4,0) tube is weaker with larger distance from the substrate and lower desorption temperature. The underlying reason is the longer Ni–N bond length due to the stress in the curved tube, which reduces the charges on Ni ions.

From above discussions, one can see that H₂ molecules can be quasi-molecularly adsorbed on the penta-NiN₂ sheet and tube, where the positively charged Ni ion produces an electric field which polarizes H₂ molecules. Such mechanism can be visualized with charge density difference as shown in Fig. 7, where one can clearly see that the charge density difference is

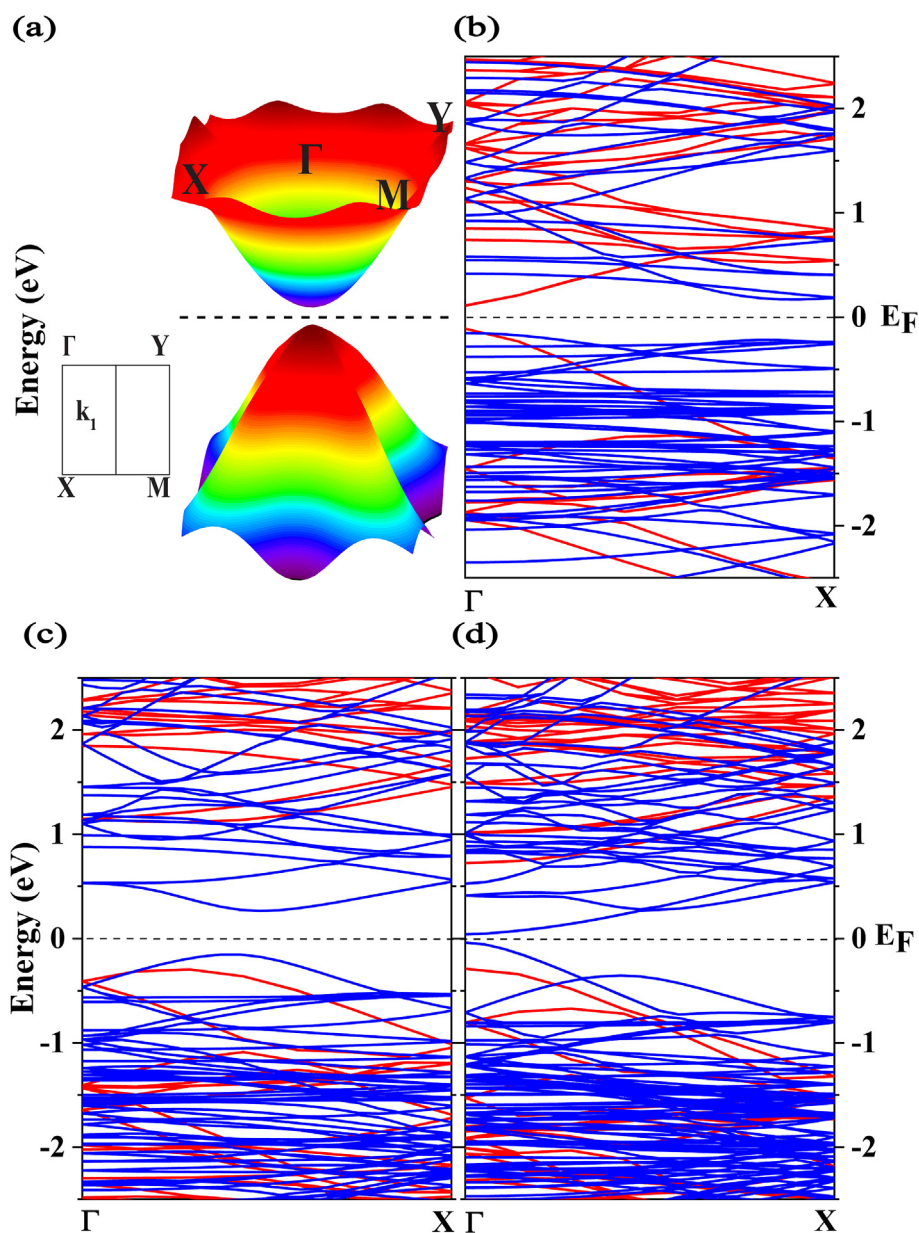


Fig. 4 – (a) Energy dispersion of the monolayer $p\text{-NiN}_2$ with the highest occupied state and lowest unoccupied states over the Brillouin zone. The electronic band structure of $p\text{-NiN}_2$ nanotubes: (b) (4, 0), (c) (5, 0), (d) (8, 0). The Fermi level is represented by a horizontal dotted line. (PBE-GGA) is represented by the blue line, while HSE06 is represented by the red line, respectively. (For interpretation of the references to colour in this figure legend, the reader is referred to the Web version of this article.)

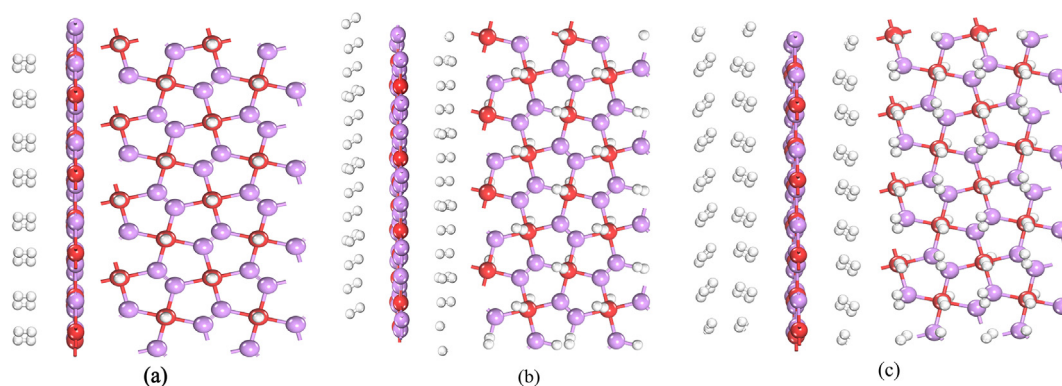


Fig. 5 – Relaxed structures (top and side views) of the adsorbed hydrogen molecules with 1–0 (a), 1–1 (b) and 2–1 (c) configurations on penta- NiN_2 sheet.

Table 2 – The average distance Ni–H₂ ($D_{\text{Ni-H}_2}$, the number in parentheses is for the second layer H₂), adsorption energy per H₂ (E_{ad}), the average charge transfer from monolayer to per H₂ molecule ($Q_{\text{gain}} n\text{H}_2$) according to Bader charge analysis, and desorption temperature (T_d).

System	Config	$D_{\text{Ni-H}_2}$ (Å)	E_{ad} (meV)	$Q_{\text{gain}} n\text{H}_2$	T_d (K)
Monolayer	1–0	2.566	102.8	–0.006	131
	1–1	2632	1021	–0.005	130
	2–1	2606 (4.97)	902	–0.003	115
Nanotube	1–0	2.808	82.1	–0.003	105
	2–0	2863	716	–0.002	90
	3–0	2.912 (5.20)	63.4	–0.002	81

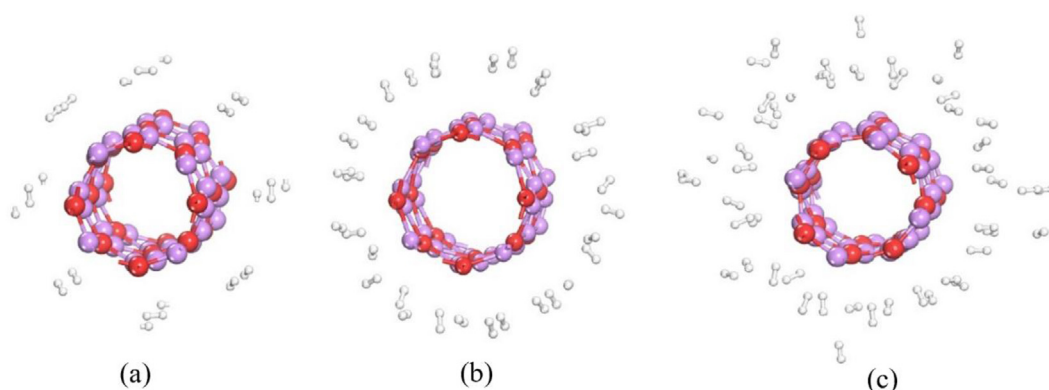


Fig. 6 – Relaxed structure of H₂ adsorption with 1–0 (a), 2–0 (b) and 3–0 (c) configuration on penta-NiN₂ (4,0) nanotube.

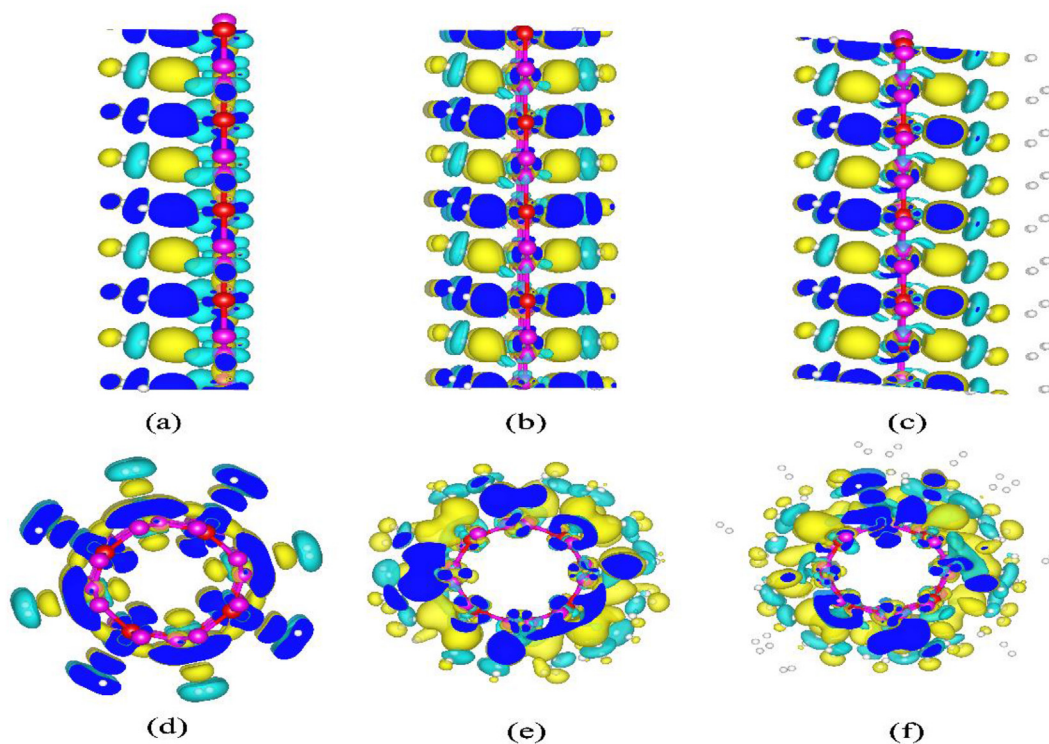


Fig. 7 – Charge density difference of H₂ adsorbed on the penta-NiN₂ sheet with 1–0 (a), 1–1 (b) and 2–1 (c) configurations, and on (4,0) nanotube with 1–0 (d), 2–0 (e), and 3–0 (f) configuration. The yellow and gray represent the accumulation and depletion of electron density, respectively. (For interpretation of the references to colour in this figure legend, the reader is referred to the Web version of this article.)

zero for the second layer of H₂ on the sheet (Fig. 7 c) and on the tube (Fig. 7 f), suggesting that the weak adsorption of the second layer of H₂ is due to the weak polarization.

Conclusion

In summary, first-principles calculations were performed to study H₂ adsorption on penta-NiN₂ sheet which was experimentally synthesized recently. For comparison, penta-NiN₂ nanotubes were also studied. The following conclusions can be obtained: (1) The positively charged Ni ions are the adsorption centers that polarize hydrogen molecules; (2) As limited by the 18-electron rule, each Ni ion can only adsorb two H₂ molecules with suitable adsorption energy that is within the required energy window, exhibiting a capacity of 4.44 wt%; (3) As the number of H₂ molecules increases, the adsorption energy reduces, accordingly, the desorption temperature decreases; (4) The H₂ adsorption on penta-NiN₂ nanotube with a small radius is weaker than the adsorption on the penta-NiN₂ sheet. In short, the perfect penta-NiN₂ sheet and tube are not suitable for H₂ storage with the required high performance, some kind of defects such as N-vacancy, Ni replacement with Sc and grain boundary need to be introduced for enhancing the adsorption energy as well as the capacity.

Declaration of competing interest

The authors declare that they have no known competing financial interests or personal relationships that could have appeared to influence the work reported in this paper.

Acknowledgments

This work was partially supported by grants from the National Key Research and Development Program of China (2021YFB4000601), and from the China Scholarship Council (CSC). The calculations were supported by the High-performance Computing Platform of Peking University.

REFERENCES

- [1] Kumar P, Singh S, Hashmi SAR, Kim KH. MXenes: emerging 2D materials for hydrogen storage. *Nano Energy* 2021;85:105989. <https://doi.org/10.1016/j.nanoen.2021.105989>.
- [2] US DOE Target Explanation Document: Onboard Hydrogen Storage for Light-Duty Fuel Cell Vehicles. <https://www.energy.gov/eere/fuelcells/doe-technical-targets-onboard-hydrogen-storage-light-duty-vehicles>.
- [3] Zhang S, Zhou J, Wang Q, Chen X, Kawazoe Y, Jena P. Penta-graphene: a new carbon allotrope. In: *Proceedings of the National Academy of Sciences*; 2015. p. 2372–7. <https://doi.org/10.1073/pnas.1416591112>. 112 .
- [4] Shen Y, Wang Q. Pentagon-based 2D materials: classification, properties and applications. *Phys Rep* 2022;964:1–42. <https://doi.org/10.1016/j.physrep.2022.03.003>.
- [5] Nazir MA, Hassan A, Shen Y, Wang Q. Research progress on penta-graphene and its related materials: properties and applications. *Nano Today* 2022;44:101501. <https://doi.org/10.1016/j.nantod.2022.101501>.
- [6] Zhang Y, Liu P, Zhu X. Li decorated penta-silicene as a high capacity hydrogen storage material: a density functional theory study. *Int J Hydrogen Energy* 2021;46:4188–200. <https://doi.org/10.1016/j.ijhydene.2020.10.193>.
- [7] Hao J, Wei F, Zhang X, Li L, Chen C, Wu G, Song H. An investigation of Li-decorated N-doped penta-graphene for hydrogen storage. *Int J Hydrogen Energy* 2021;46:25533–42. <https://doi.org/10.1016/j.ijhydene.2021.05.089>.
- [8] Shajahan AS, Kalarikkal N, Garg N, Kawazo Y, Chakraborty B. A quest to high-capacity hydrogen storage in zirconium decorated pentagraphene: DFT perspectives. *Int J Hydrogen Energy* 2022;47:36190–203. <https://doi.org/10.1016/j.ijhydene.2022.08.172>.
- [9] Bi L, Miao Z, Ge Y, Liu Z, Xu Y, Yin J, Yang Z. Density functional theory study on hydrogen storage capacity of metal-embedded penta-octa-graphene. *Int J Hydrogen Energy* 2022;47:32552–64. <https://doi.org/10.1016/j.ijhydene.2022.07.134>.
- [10] Ma LJ, Gao SQ, Jia JF, Wu HS. Effects of charging, strain, and doping on the interaction between H₂ and nitrogen-rich Penta-CN₂ sheet. *Int J Hydrogen Energy* 2022;47:34183–94. <https://doi.org/10.1016/j.ijhydene.2022.08.020>.
- [11] Bykov M, Bykova E, Ponomareva AV, Tasnadi F, Chariton S, Prakupenka VB, Glazyrin K, Smith JS, Mahmood MF, Abrikosov IA, Goncharov AF. Realization of an ideal cairo tessellation in nickel diazenide NiN₂: high-pressure route to pentagonal 2D materials. *ACS Nano* 2021;15:13539–46. <https://doi.org/10.1021/acsnano.1c04325>.
- [12] Shin WH, Yang SH, Goddard III WA, Kang JK. Ni-dispersed fullerenes: hydrogen storage and desorption properties. *Appl Phys Lett* 2006;88:053111. <https://doi.org/10.1063/1.2168775>.
- [13] Venkataramanan NS, Khazaee M, Sahara R, Mizuseki H, Kawazoe Y. First-principles study of hydrogen storage over Ni and Rh doped BN sheets. *Chem Phys* 2009;359:173–8. <https://doi.org/10.1016/j.chemphys.2009.04.001>.
- [14] Shalabi AS, El Mahdy AM, Soliman KA, Taha HO. Theoretical characterisation of irreversible and reversible hydrogen storage reactions on Ni-doped C60 fullerene. *Mol Phys* 2014;112:3057–71. <https://doi.org/10.1080/00268976.2014.928754>.
- [15] El Mahdy AM, Taha HO, Kamel MA, El Shemy F. Theoretical study of hydrogen storage reactions on nickel-decorated heterofullerene C₅₈ B_XN_Y (X+Y= 2). *Mol Phys* 2018;116:2321–42. <https://doi.org/10.1080/00268976.2018.1483536>.
- [16] Goudarziafshar H, Abdolmaleki M, Moosavi-zare AR, Soleymanabadi H. Hydrogen storage by Ni-doped silicon carbide nanocage: a theoretical study. *Phys E Low-dimens Syst Nanostruct* 2018;101:78–84. <https://doi.org/10.1016/j.physe.2018.03.001>.
- [17] Taha HO, Tarek MA. Axial deformation effects on hydrogen storage of Ni decorated (8, 0) zigzag single-walled boron nitride nanotubes: a DFT study. *Mol Phys* 2021;119:e1937738. <https://doi.org/10.1080/00268976.2021.1937738>.
- [18] Kireev NV, Kiryutin AS, Pavlov AA, Yurkovskaya AV, Musina EI, Karasik AA, Elena S Sh, Ivanov KL, Belkova NV. Nickel (II) dihydrogen and hydride complexes as the intermediates of H₂ heterolytic splitting by nickel diazadiphosphacyclooctane complexes. *Eur J Inorg Chem* 2021;41:4265–72. <https://doi.org/10.1002/ejic.202100489>.
- [19] Kresse G, Furthmüller J. Efficient iterative schemes for ab initio total-energy calculations using a plane-wave basis set. *Phys Rev B* 1996;54:11169. <https://doi.org/10.1103/PhysRevB.54.11169>.

- [20] Perdew J. P., Burke K., Ernzerhof M. Generalized gradient approximation made simple. *Phys Rev Lett* 1996; 77: 3865. <https://doi.org/10.1103/PhysRevLett.77.3865>.
- [21] Kresse G, Joubert D. From ultrasoft pseudopotentials to the projector augmented-wave method. *Physical review b* 1999;59:1758. <https://doi.org/10.1103/PhysRevB.59.1758>.
- [22] Heyd J, Scuseria GE. Efficient hybrid density functional calculations in solids: assessment of the Heyd–Scuseria–Ernzerhof screened Coulomb hybrid functional. *J Chem Phys* 2004;121:1187–92. <https://doi.org/10.1063/1.1760074>.
- [23] Grimme S, Antony J, Ehrlich S, Krieg H. A consistent and accurate ab initio parametrization of density functional dispersion correction (DFT-D) for the 94 elements H–Pu. *J Chem Phys* 2010;132:154104. <https://doi.org/10.1063/1.3382344>.
- [24] Monkhorst HJ, Pack JD. Special points for Brillouin-zone integrations. *Phys Rev B* 1976;13:5188. <https://doi.org/10.1103/PhysRevB.13.5188>.
- [25] Liu J, Cheng B. New understanding of photocatalytic properties of zigzag and armchair g-C₃N₄ nanotubes from electronic structures and carrier effective mass. *Appl Surf Sci* 2018;430:348–54. <https://doi.org/10.1016/j.apsusc.2017.06.205>.
- [26] Zhao Y, Kim YH, Dillon AC, Heben MJ, Zhang SB. Hydrogen storage in novel organometallic buckyballs. *Phys Rev Lett* 2005;94:155504. <https://doi.org/10.1103/PhysRevLett.94.155504>.
- [27] Kiran B, Kandalam AK, Jena P. Hydrogen storage and the 18-electron rule. *J Chem Phys* 2006;124:224703. <https://doi.org/10.1063/1.2202320>.
- [28] Crabtree RH. *The organometallic chemistry of the transition metals*. John Wiley & Sons; 2009.
- [29] Ma LJ, Sun Q. A topological semimetal Li₂CrN₂ sheet as a promising hydrogen storage material. *Nanoscale* 2020;12:12106–13. <https://doi.org/10.1039/D0NR02180F>.
- [30] Jindal R, Sharma V, Shukla A. Density functional theory study of the hydrogen evolution reaction in haeckelite boron nitride quantum dots. *Int J Hydrogen Energy* 2022;47:41783–94. <https://doi.org/10.1016/j.ijhydene.2022.06.216>.
- [31] Dewangan J, Mahamiya V, Shukla A, Chakraborty B. Lithium decorated Ψ-graphene as a potential hydrogen storage material: density functional theory investigations. *Int J Hydrogen Energy* 2022. <https://doi.org/10.1016/j.ijhydene.2022.10.142>.
- [32] Durgun E, Ciraci S, Yildirim T. Functionalization of carbon-based nanostructures with light transition-metal atoms for hydrogen storage. *Phys Rev B* 2008;77:085405. <https://doi.org/10.1103/PhysRevB.77.085405>.
- [33] Mishra P, Singh D, Sonvane Y, Ahuja R. Metal-functionalized 2D boron sulfide monolayer material enhancing hydrogen storage capacities. *J Appl Phys* 2020;127:184305. <https://doi.org/10.1063/5.0008980>.
- [34] Hu S, Yong Y, Zhao Z, Gao R, Zhou Q, Kuang Y. C₇N₆ monolayer as high capacity and reversible hydrogen storage media: a DFT study. *Int J Hydrogen Energy* 2021;46:21994–2003. <https://doi.org/10.1016/j.ijhydene.2021.04.053>.
- [35] Petrushenko IK, Bettinger HF. Hydrogen adsorption on inorganic benzenes decorated with alkali metal cations: theoretical study. *Phys Chem Chem Phys* 2021;23:5315–24. <https://doi.org/10.1039/D1CP00025J>.
- [36] Chettri B, Patra PK, Srivastava S, Laref A, Rai DP. Enhanced H₂ storage capacity of bilayer hexagonal boron nitride (h-BN) incorporating van der Waals interaction under an applied external electric field. *ACS Omega* 2021;6:22374–82. <https://doi.org/10.1021/acsomega.1c03154>.
- [37] Yuan JH, Song YQ, Chen Q, Xue KH, Miao XS. Single-layer planar penta-X₂N₄ (X= Ni, Pd and Pt) as direct-bandgap semiconductors from first principle calculations. *Appl Surf Sci* 2019;469:456–62. <https://doi.org/10.1016/j.apsusc.2018.11.041>.